JACS
JOURNAL OF THE AMERICAN CHEMICAL SOCIETY

Communication

pubs.acs.org/JACS

Phase-Pure $FeSe_x$ (x = 1, 2) Nanoparticles with One- and Two-Photon Luminescence

Xiang Mao,[†] Jin-Gyu Kim,[‡] Jishu Han,[§] Hyun Suk Jung,[‡] Sang Gil Lee,[‡] Nicholas A. Kotov,*[,§] and Jaebeom Lee*[,†]

[†]Department of Nano Fusion Engineering and Cogno-Mechatronics Engineering, Pusan National University, Busan 609-735 Republic of Korea

[‡]Division of Electron Microscopic Research, Korea Basic Science Institute, Daejeon 350-806, Republic of Korea

[§]Department of Chemical Engineering, University of Michigan, Ann Arbor, Michigan 48109, United States

Supporting Information

ABSTRACT: Iron chalcogenides hold considerable promise for energy conversion and biomedical applications. Realization of this promise has been hindered by the lack of control over the crystallinity and nanoscale organization of iron chalcogenide films. High-quality nanoparticles (NPs) from these semiconductors will afford further studies of photophysical processes in them. Phase-pure NPs from these semiconductors can also serve as building blocks for mesoscale iron chalcogenide assemblies. Herein we report a synthetic method for $FeSe_x$ (x = 1, 2) NPs with a diameter of ca. 30 nm that satisfy these needs. The high crystallinity of the individual NPs was confirmed by transmission electron microscopy (TEM) and energy-dispersive X-ray analysis. TEM tomography images suggest pucklike NP shapes that can be rationalized by bond relaxation at the NP edges, as demonstrated in large-scale atomic models. The prepared $FeSe_x$ NPs display strong photoluminescence with a quantum yield of 20%, which was previously unattainable for iron chalcogenides. Moreover, they also show strong off-resonant luminescence due to two-photon absorption, which should be valuable for biological applications.

Over the past decade, nanoparticles (NPs) from transition-metal chalcogenides have received widespread attention because of their electronic and optical properties. Various applications include photovoltaics, thermoelectric memory, electronic devices, biological tags, sensors, and others.[1−3] Both fundamental and applied research has been primarily carried out on NPs of II−VI semiconductors, such as chalcogenides of Cd, Zn, and Hg.[4−6] Much less attention has been given to chalcogenides of Fe, possibly because of discouraging results regarding their past use in photovoltaics[7a] and weak luminescence. Other factors that have further diminished the research interest in NPs from iron chalcogenides compared with, for example, cadmium chalcogenides include poor phase purity and crystallinity of the iron-based semiconductors.[7b] On the other hand, the uniquely high earth abundance and low toxicity of iron can be a considerable advantage of iron chalcogenides in energy conversion[7c,d] and photo- and electrocatalysis applications.[10a] Nanoscale FeSe is also attractive as a superconducting material.[8] Despite auspicious animal tests of the use of Cd- and Pb-based NPs for imaging, concerns about their toxicity remain.[9] Among all semiconductor materials, iron chalcogenides can cause the least possible toxicity and therefore would be favorites for biological applications should the problem with their weak luminescence be resolved.

High-quality single-crystalline NPs, nanowires, and nanosheets were recently made from FeS, but their luminescence was still weak.[10] Chalcogenides with larger molecular mass may exhibit stronger luminescence and more interesting optical properties. Iron selenide exists in two stoichiometric ratios: FeSe and $FeSe_2$.[11a] FeSe crystallizes in tetragonal and hexagonal forms, while $FeSe_2$ crystallizes in cubic and orthorhombic (marcasite-type) phases.[11b] FeSe has a direct band gap of 1.23 eV and an absorption coefficient of 5×10^5 cm^{-1} for λ <800 nm. $FeSe_2$ is known to have indirect band gaps of 0.86 and 0.67 eV in the marcasite and pyrite phases, respectively.[12,13a] Taken together, these data motivated us to develop new methods for the synthesis of iron selenide NPs. There have been no reports of iron chalcogenide NPs with reasonably strong luminescence (quantum yield greater than 10%). Besides their low phase purity, the lack of fluorescence should be attributed to an unfavorable band gap structure[13b] and insufficient passivation.

In this paper, we describe the synthesis of FeSe and $FeSe_2$ NPs stabilized by 1-octadecene (ODE) and oleic acid (OA). Initially, we made two different constitutive solutions. For solution A, 0.04 mM iron(II) acetylacetonate [$Fe(acac)_2$] and OA were dissolved in ODE at 120 °C until the mixture changed from yellow to colorless. For solution B, 0.04 mM Se micropowder was dissolved in ODE at 120 °C. The synthesis of $FeSe_x$ (x = 1, 2) NPs was carried out by dropwise addition of solution A (preheated to 120 °C) to solution B at 330 °C with vigorous stirring for 0.5 h. To obtain FeSe and $FeSe_2$ NPs, we used 1 mL and 2 mL of solution B, respectively [see Scheme S1 in the Supporting Information (SI)]; 1:1 and 1:2 ratios of solutions A and B gave FeSe and $FeSe_2$ NPs, respectively (see below). We believe that ODE, in addition to its role as the solvent, acts as a coordinating agent to iron ions on the surface of the NPs. OA strongly coordinates with iron atoms via its carboxyl group.[14] The combination of two capping agents, one weak and one

Received: December 18, 2013
Published: March 26, 2014

   dx.doi.org/10.1021/ja412654c | J. Am. Chem. Soc. 2014, 136, 7189−7192

strong, was proven to be useful for a number of semiconducting particles and can be investigated further to improve the monodispersity in the study of these NP syntheses.[15]

The purified $FeSe_x$ NPs were obtained by heating the mixed precursors for 1.5 h at 330 °C. The solutions turned from yellow to colorless when the iron precursors were mixed in ODE and heated, and they finally became yellow (UV peak at 317 nm) and brown-yellow (UV peak at 324 nm) for FeSe and $FeSe_2$, respectively. In contrast to syntheses employing other surfactants,[16] no microscale precipitates appeared in this method. The final products were collected from the inner wall of the glass flask.[17] The NPs were subsequently purified by the precipitation−redispersion technique (see the SI). Iron chalcogenide NPs are prone to form disorganized precipitates,[18] but this was not observed for our method. We obtained stable dispersions, typical for the high-temperature organometallic route.[19] The average diameter of the FeSe NPs (36 ± 4 nm) was slightly larger than that of the $FeSe_2$ NPs (32 ± 5 nm) (Figure S2 in the SI). The NPs were characterized by high-resolution transmission electron microscopy (HRTEM). Figure 1 shows TEM images of

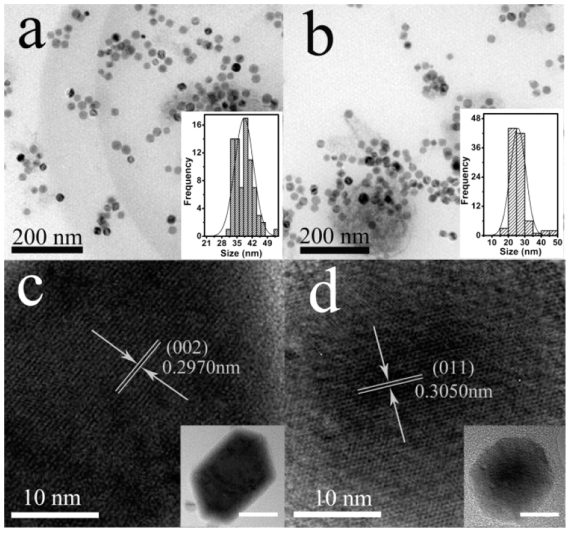

Figure 1. TEM images of (a) FeSe and (b) $FeSe_2$ (insets: size distributions of NPs in the TEM images) and HRTEM images of the (c) FeSe and (d) $FeSe_2$ NPs shown in the inset images. Scale bars in the insets are 15 nm.

the synthesized $FeSe_x$ NPs with corresponding size distributions (insets in Figure 1a,b). To investigate the parameter space for the synthesis of these NPs a bit more, we also carried out the synthesis using different reaction times and obtained TEM images for each reaction (Figure S3). HRTEM showed crystal lattice spacings of 0.297 and 0.305 nm for FeSe(002) and $FeSe_2$(011), respectively (Figure 1c,d). The elemental composition of the NPs was analyzed by energy-dispersive X-ray (EDX) analysis. NPs with Fe:Se ratios of 1:1.05 and 1:2.17 were attributed to FeSe and $FeSe_2$, respectively (Figure S4). Quantification of the EDX spectra was based on a statistical analysis of compositions obtained for more than 50 NPs in different locations.

The X-ray diffraction (XRD) pattern of the FeSe NPs was assigned using the peaks indexed to the PbO-type tetragonal α-FeSe phase (JCPDS no. 03-0533). The XRD pattern of $FeSe_2$ NPs was indexed to the orthorhombic ferroselite structure (JCPDS no. 21-0432), which we believe is the closest fit in this case (Figure 2). Notably, there are substantial deviations in the XRD peaks with ferroselite. The HRTEM images revealed that

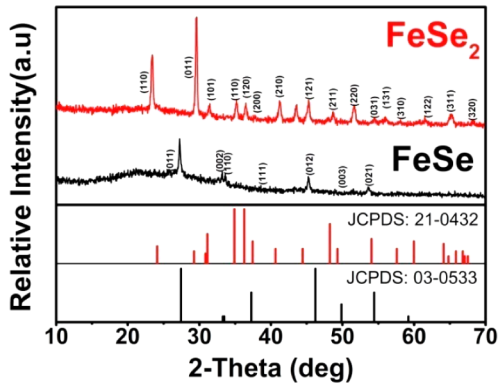

Figure 2. XRD patterns of the FeSe NPs (black curves) and $FeSe_2$ NPs (red curves).

the spacing between adjacent lattice fringes corresponds to the interplanar distances of the (002) and (011) planes for the FeSe and $FeSe_2$ NPs, respectively.[20]

The particle shapes were investigated by three-dimensional (3D) TEM tomography (Figure 3g−i for FeSe and Figure 3j−l

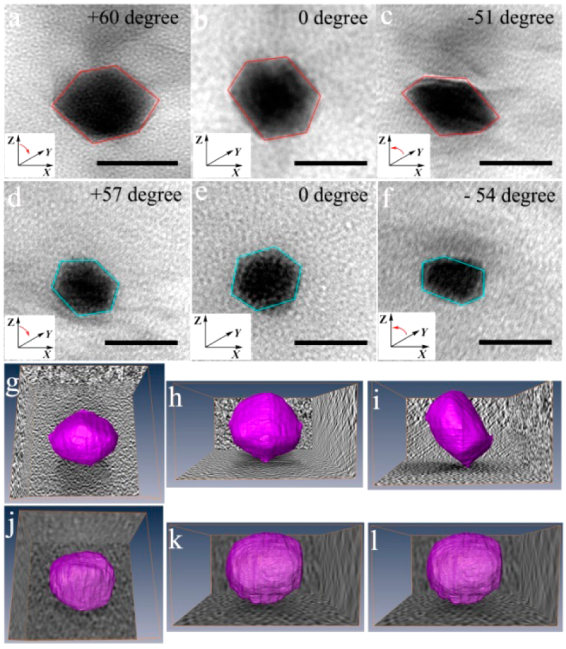

Figure 3. (a−c) TEM images of FeSe NPs taken at tilt angles of +60°, 0°, and −51° between the *y* and *z* axes, respectively, where *x* is the sample rotation axis and *y* is the electron beam irradiation axis. (d−f) TEM images of $FeSe_2$ NPs taken at tilt angles of +57°, 0°, and −54°, respectively. The scale bars are 50 nm. (g−l) 3D renderings of single (g−i) FeSe and (j−l) $FeSe_2$ NPs obtained by TEM tomography (also see the video files in the SI).

for $FeSe_2$) based on a series of acquired bright-field TEM images ranging from −51° to +60° (FeSe) and −54° to +57° ($FeSe_2$) in tilt steps of 3° at 120 kV with zero-loss filtering. A total of 38 single-axis tilt-series TEM images were obtained. 3D rendering of the TEM data provides different views from several axes (also see the video files in the SI). The particle sizes of different NPs were in agreement with the TEM results shown in Figure 1. Their

dx.doi.org/10.1021/ja412654c | J. Am. Chem. Soc. 2014, 136, 7189−7192

geometrical shapes can be described as pucklike polygons. Perfect hexagons or other precisely defined polygonal shapes are difficult to expect from these nanocrystals in TEM images, despite their high XRD crystallinity, because of the relaxation of chemical bonds at the NP edges due to the fairly weak geometrical constraints imposed on the lattice by ODE and OA. Thermodynamically driven relaxation of the bonds also leads to the "rounding" of the shapes that can be also seen in the large-scale atomic simulations of the NPs carried out in the approximation of elastic behavior of all the bonds (Figure 4).

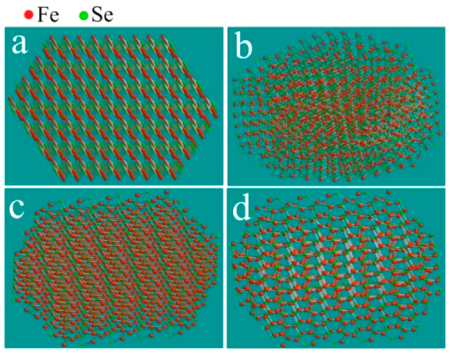

Figure 4. Simulated shapes of (a, b) FeSe and (c, d) $FeSe_2$ NPs (a, c) before and (b, d) after energy minimization of the atomic lattices.

Minimization of the energy of the atoms at the interfaces results in edge-softening as observed in the TEM images. Although quite simple, the molecular mechanics MMFF algorithm is well-suited for the description of NP shapes. One of the advantages of this method is its suitability to the large number of atoms needed to adequately describe NPs of reasonably large size. The atomic system described here consists of more than 2300 atoms and corresponds to an NP with a long axis of 4.2 nm.

The optical properties of FeSe and $FeSe_2$ in *n*-hexane dispersions were evaluated at room temperature. The absorption bands for both FeSe and $FeSe_2$ NPs revealed maxima at 320 nm (Figure 5a). The band gaps for both types of NPs were estimated using the standard methods based on absorption spectra (Figure S5).[21] The band gaps for $FeSe_x$ NPs were estimated to be between 2.25 and 2.51 eV by performing the Kubelka–Munk transformation.[17b,21a–c] Even the lower threshold of this estimate is greater than the values reported in other studies.[22] This is indicative of greater quantum confinement, which can increase the electron–hole radiative recombination probability and fluorescence quantum yield provided that there are no charge traps within the NPs to stimulate nonradiative recombination.

Strong photoluminescence (PL) bands were found at λ_{PL} = 447 and 462 nm for FeSe and $FeSe_2$ NPs, respectively, upon excitation at λ_{ex} = 365 nm (Figure 5b). The emission bands for both types of NPs are relatively wide with full widths at half-maximum (fwhm) of over 100 nm, which is mainly attributed to the NP size distribution. The PL properties during the growth process of the NPs were also investigated. As expected, a gradual red shift of the PL spectra occurs with increasing reaction time, corresponding to NP growth (Figure S6). This observation confirms the attribution of the emission bands to the NPs rather than to organometallic compounds of iron (and it should also be noted that most of the impurities were removed during the process of dispersion preparation). The PL lifetimes (τ) were 3.07 ± 0.02 ns for FeSe and 2.54 ± 0.02 ns for $FeSe_2$ (Figure 5c), which are typical of NPs. The quantum yields (QYs) of the NPs

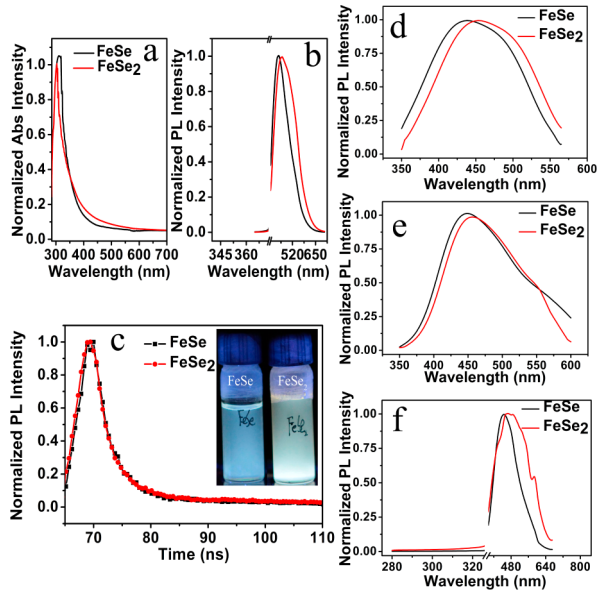

Figure 5. (a) UV–vis absorption and (b) PL spectra of FeSe and $FeSe_2$ NPs. (c) Luminescence decay of FeSe (black) and $FeSe_2$ (red) NPs. The inset is a photograph of NP dispersions under UV irradiation. (d–f) Off-resonance luminescence spectra of FeSe (black) and $FeSe_2$ (red) NPs from two-photon absorption at different excitation wavelengths: (d) 600 nm; (e) 650 nm; (f) 700 nm.

were 20% for FeSe and 16% for $FeSe_2$ (see the SI). Typically, chalcogenide NPs without a wide-band-gap shell have been reported to have QYs of 10–40%.[23a] It was unexpected that iron chalcogenide NPs would display QYs comparable to those of II–VI semiconductors. In the past we were not able to observe strong PL in pyrite (FeS_2),[10a] nor could other researchers for similar compounds.[10b] The non-Lorentzian shape of the emission bands is indicative of a complex emission pattern with, most likely, multiple emitting states. Some of these states are likely to be related to the relaxed atomic lattice on the outer edges of the NPs (Figure 4). The crystal lattice relaxation on the NP surface may also result in additional exciton confinement. It was different with previous Au clusters integrated within ligands, which readily showed bright fluorescence due to charge transfer between the ligands and metal atoms.[23b,c]

Importantly, strong emission of both types of NPs was also observed upon illumination by the photons with energies lower than the band gap (Figure 5d–f). We used excitation light at λ_{ex} = 600, 650, and 700 nm and observed the emission at $\lambda_{2PL} \approx$ 430 and 450 nm for FeSe and $FeSe_2$ NPs, respectively. The shapes and positions of the peaks were similar to those for illumination at λ_{ex} = 365 nm. The appearance of these peaks is attributed to the unusually strong two-photon absorption that was previously observed for CdTe NPs.[23d–g] This phenomenon was suggested as a convenient tool for deep-tissue imaging with IR photons, which have a much better penetration range into tissue. However, the toxicity of CdTe is a valid concern in this case.[23g] The $FeSe_x$ NPs reveal a similar luminescence intensity for two-photon absorption. The biocompatibility of iron in place of cytotoxic Cd makes these NPs promising substitutes for biomedical fluorescence tags. The significance of such tags for cancer imaging has been recently demonstrated.[24] The favorable toxicological properties make the $FeSe_x$ NPs attractive also for optical, electronic, and photovoltaic materials, particularly for implantable devices.[25]

dx.doi.org/10.1021/ja412654c | J. Am. Chem. Soc. 2014, 136, 7189–7192

■ ASSOCIATED CONTENT

Supporting Information

Experimental details, TEM and TGA data, and optical spectra. This material is available free of charge via the Internet at http://pubs.acs.org.

■ AUTHOR INFORMATION

Corresponding Authors

kotov@umich.edu
jaebeom@pusan.ac.kr

Notes

The authors declare no competing financial interest.

■ ACKNOWLEDGMENTS

This study was supported by grants from the Korea Healthcare Technology R&D Project (A110191) of the Ministry for Health, Welfare & Family Affairs and the Basic Science Research Program through the National Research Foundation of Korea (NRF) funded by the Ministry of Education (2013004637). This study was partially supported by the Center for Solar and Thermal Energy Conversion, an Energy Frontier Research Center under the auspices of the U.S. Department of Energy, Office of Science, Office of Basic Energy Sciences under Award DE-SC0000957. We acknowledge support from NSF under Grants ECS-0601345, EFRI-BSBA 0938019, CBET 0933384, CBET 0932823, and CBET 1036672. This work was also partially supported by ARO MURI W911NF-12-1-0407 "Coherent Effects in Hybrid Nanostructures for Lineshape Engineering of Electromagnetic Media" (N.A.K.).

■ REFERENCES

(1) Zhou, Y.; Zhu, Z.; Huang, W.; Liu, W.; Wu, S.; Liu, X.; Gao, Y.; Zhang, W.; Tang, Z. *Angew. Chem.* **2011**, *123*, 11658.

(2) (a) Zhou, Y.; Yang, M.; Sun, K.; Tang, Z.; Kotov, N. A. *J. Am. Chem. Soc.* **2010**, *132*, 6006. (b) Wang, J. J.; Xue, D. J.; Wan, L. J. *J. Am. Chem. Soc.* **2011**, *133*, 18558.

(3) (a) Wang, Y. H.; Bao, N.; Shen, L.; Padhan, P.; Gupta, A. *J. Am. Chem. Soc.* **2007**, *129*, 12408. (b) Kumar, S.; Nann, T. *Small* **2006**, *2*, 316. (c) Rao, C. N. R.; Deepak, F. L.; Gundiah, G.; Govindaraj, A. *Prog. Solid State Chem.* **2003**, *31*, 5.

(4) (a) Xiong, S.; Xi, B.; Wang, W.; Qian, Y. *Chem.—Eur. J.* **2007**, *13*, 3076. (b) Moore, D.; Wang, Z. L. *Angew. Chem., Int. Ed.* **2006**, *45*, 5150. (c) Zeng, R.; Zou, B. *J. Phys. Chem. C* **2011**, *115*, 3005.

(5) (a) Yang, S. L.; Yao, H. B.; Gao, M. R.; Yu, S. H. *CrystEngComm* **2009**, *11*, 1383. (b) Gao, F.; Lu, Q.; Zhao, D. *Nano Lett.* **2003**, *3*, 85.

(6) Freeman, J. W.; Basolo, F. *J. Am. Chem. Soc.* **1991**, *113*, 6509.

(7) (a) Ennaoui, A.; Tributsch, H. *Sol. Cells* **1984**, *13*, 197. (b) Tamaki, Y.; Asahi, T.; Masuhara, H. *J. Phys. Chem. A* **2002**, *106*, 2135. (c) Zhang, G.; Fang, H.; Wu, Y. *Nano Lett.* **2012**, *12*, 3627. (d) Lucas, J. M.; Lanzara, A.; Alivisatos, A. P. *Chem. Mater.* **2013**, *25*, 1615.

(8) Mizuguchi, Y.; Takano, Y. *Appl. Phys. Lett.* **2008**, *93*, No. 152505.

(9) (a) Fan, K.; Cao, C.; Yan, X. *Nat. Nanotechnol.* **2012**, *7*, 459. (b) Ghosh, D.; Kelly, K. A. *Nat. Nanotechnol.* **2012**, *7*, 677.

(10) (a) Bai, Y.; Sun, K.; Kotov, N. A. *J. Phys. Chem. C* **2013**, *117*, 2567. (b) Cabán-Acevedo, M.; Jin, S. *Nano Lett.* **2012**, *12*, 1977.

(11) (a) Kumar, R. S.; Zhang, Y.; Cornelius, A. L.; Chen, C. *J. Phys. Chem. B* **2010**, *114*, 12597. (b) Akhtar, M.; Akhtar, J.; Malik, M. A.; Tuna, F.; Helliwell, M.; O'Brien, P. *J. Mater. Chem.* **2012**, *22*, 14970.

(12) (a) Yuan, B.; Luan, W.; Tu, S. T. *New J. Chem.* **2012**, *36*, 2101. (b) Ganga, B. G.; Santhosh, P. N. arXiv:1303.1381v1, 2013.

(13) (a) Thanikaikarasan, S.; Mahalingam, T.; Kim, T. *Vacuum* **2009**, *83*, 1066. (b) Chikan, V.; Kelley, D. F. *Nano Lett* **2002**, *2*, 141.

(14) Sun, S.; Zeng, H. *J. Am. Chem. Soc.* **2002**, *124*, 8204.

(15) (a) Shevchenko, E. V.; Talapin, D. V.; Kotov, N. A.; O'Brien, S.; Murray, C. B. *Nature* **2006**, *439*, 55. (b) Talapin, D. V.; Murray, C. B. *Science* **2005**, *310*, 86.

(16) Wang, Y. H.; Gupta, A. *J. Am. Chem. Soc.* **2007**, *129*, 12408.

(17) (a) Gu, Y. P.; Cui, R.; Pang, D. W. *J. Am. Chem. Soc.* **2011**, *134*, 79. (b) Vaughn, D. D., II; Patel, R. J.; Hickner, M. A.; Schaak, R. E. *J. Am. Chem. Soc.* **2010**, *132*, 15170.

(18) (a) Wadia, C.; Alivisatos, A. P. *Chem. Mater.* **2009**, *21*, 2568. (b) Wang, D.-W.; Wang, Q.-H.; Wang, T.-M. *CrystEngComm* **2010**, *12*, 755.

(19) (a) Murray, C. B.; Bawendi, M. G. *Science* **1995**, *270*, 1335. (b) Talapin, D. V.; Weller, H. *Nano Lett.* **2001**, *1*, 207. (c) Qu, L.; Peng, X. *Nano Lett* **2001**, *1*, 333. (d) Peng, Z. A.; Peng, X. *J. Am. Chem. Soc.* **2002**, *124*, 3343−3353.

(20) (a) Kim, D.; Kim, B. K. *Mater. Lett.* **2006**, *60*, 2807. (b) Ramesha, K.; Seshadri, R. *Solid State Sci.* **2004**, *6*, 841.

(21) (a) Wang, J. J.; Wan, L. J. *J. Am. Chem. Soc.* **2011**, *133*, 18558. (b) Hagfeldt, A.; Grätzel, M. *Chem. Rev.* **1995**, *95*, 49. (c) Li, L.; Chen, Z.; Wang, Q. *J. Am. Chem. Soc.* **2013**, *135*, 1213. (d) Dong, F.; Wang, H.; Wu, Z. *J. Phys. Chem. C* **2009**, *113*, 16717.

(22) (a) Akhtar, M.; Akhter, J.; Malik, M. A.; O'Brien, P.; Tuna, F.; Raftery, J.; Helliwell, M. *J. Mater. Chem.* **2011**, *21*, 9737. (b) Wang, Y.; Yin, Y. *Inorg. Chem.* **2010**, *49*, 6601. (c) Xu, J.; Son, S. U. *Cryst. Growth Des.* **2011**, *11*, 2707.

(23) (a) Hines, M. A.; Guyot-Sionnest, P. *J. Phys. Chem.* **1996**, *100*, 468. (b) Mali, B.; Dragan, A. I.; Karolin, J.; Geddes, C. D. *J. Phys. Chem. C* **2013**, *117*, 16650. (c) Kawasaki, H.; Yamamoto, H.; Fujimori, H.; Arakawa, R.; Iwasaki, Y.; Inada, M. *Langmuir* **2010**, *26*, 5926. (d) Khatei, J.; Koteswara Rao, K. S. R. *Appl. Phys. Lett.* **2012**, *100*, No. 081901. (e) Dancus, I.; Eychmüller, A. *Opt. Lett.* **2010**, *35*, 1079. (f) Padilha, L. A.; Cruz, C. H. *Opt. Express* **2005**, *13*, 6460. (g) Maestro, L. M.; Jaque, D. *Nanoscale* **2012**, *4*, 298.

(24) Yu, J. H.; Na, H. B. *Nat. Mater.* **2013**, *12*, 359.

(25) Kotov, N. A.; Lieber, C. M.; Prato, M. *Adv. Mater.* **2009**, *21*, 3970.